



**HAL**  
open science

# A Graphene Oxide–Thioamide Polymer Hybrid for High-Performance Supercapacitor Electrodes

Włodzimierz Czepa, Samanta Witomska, Paolo Samorì, Artur Ciesielski

## ► To cite this version:

Włodzimierz Czepa, Samanta Witomska, Paolo Samorì, Artur Ciesielski. A Graphene Oxide–Thioamide Polymer Hybrid for High-Performance Supercapacitor Electrodes. *Small Science*, 2023, 3 (5), 10.1002/smssc.202300013 . hal-04100612

**HAL Id: hal-04100612**

**<https://hal.science/hal-04100612>**

Submitted on 17 May 2023

**HAL** is a multi-disciplinary open access archive for the deposit and dissemination of scientific research documents, whether they are published or not. The documents may come from teaching and research institutions in France or abroad, or from public or private research centers.

L'archive ouverte pluridisciplinaire **HAL**, est destinée au dépôt et à la diffusion de documents scientifiques de niveau recherche, publiés ou non, émanant des établissements d'enseignement et de recherche français ou étrangers, des laboratoires publics ou privés.

# A Graphene Oxide–Thioamide Polymer Hybrid for High-Performance Supercapacitor Electrodes

Włodzimierz Czepa, Samanta Witomska, Paolo Samorì,\* and Artur Ciesielski\*

The controlled chemical functionalization of graphene oxide (GO) represents a powerful strategy to finely tune its physical and chemical properties toward applications in energy storage. Herein, an unprecedented approach for the GO modification with thioamide-based polymers featuring numerous heteroatoms (S,N,O) is reported, which is instrumental for achieving superior electrochemical performance in symmetric supercapacitors. While the electrochemical investigations in aqueous electrolytes reveal specific capacitance of  $221 \text{ F g}^{-1}$  at  $1 \text{ A g}^{-1}$ , the use of organic media allows the specific capacitance to be boosted up to  $340 \text{ F g}^{-1}$ . Additionally, the increase of operating window yields energy densities as high as  $94.4 \text{ Wh kg}^{-1}$ , thereby exceeding state-of-the-art performances of GO-based supercapacitors. Furthermore, the symmetric devices exhibit great robustness in both aqueous and organic electrolytes as evidenced by an excellent stability after 5000 working cycles ( $>98\%$  in  $\text{H}_2\text{SO}_4$  and  $>90\%$  in  $\text{TEABF}_4/\text{ACN}$ ).

## 1. Introduction

The ever-growing energy needs call for the development of new power sources and sustainable energy storage systems. Supercapacitors (SCs) represent an attractive portable energy storage alternative to state-of-the-art devices, e.g., batteries, as they combine very high cycling stability, ultrafast charging, high range of operating temperatures and improved durability, and most importantly high power density.<sup>[1–3]</sup> However, several

obstacles need to be overcome to render SCs ready for being used in daily applications, e.g., to power portable electronic devices. The existing major problems to be solved include: 1) the lack of industrial standardization such as general specifications, electrodes, and electrolyte specifications; 2) low rated voltages, which require preparation of stack of connected SC components for practical applications; 3) relative low energy densities, which result in the need of constructing bulky, noncompact, and relatively heavy devices.<sup>[4,5]</sup> Various types of materials have been investigated for application in energy storage devices exploiting either their electrochemical double-layer (ECDL) formation or pseudocapacitance (PS) provided by Faradic reactions taking place on redox active sites on

electrode–electrolyte interface.<sup>[6–9]</sup> In this context, different forms of carbon-based materials including activated carbon, carbon nanotubes, and graphene-based materials have been studied in the last decade.<sup>[10–12]</sup> To enhance their electrochemical characteristics, these materials have been modified by increasing their porosity, which rules the electrolyte penetration within the electrode material and therefore it allows control over the kinetics of charge/discharge processes. Moreover, to provide additional pseudocapacitive behaviors, heteroatoms such as N, P, S, and O have been introduced.<sup>[13–15]</sup> During the last few years, numerous studies have been reported on the exploration of 2D materials toward enhanced efficiency in energy storage density, mainly achieved by increasing their specific surface areas, taking advantage of their high electrical conductivity, and by developing synthetic protocols that can be potentially upscaled.<sup>[16,17]</sup>

Among 2D materials, graphene oxide (GO) can be produced in large scale at moderate costs, and it is known to exhibit unique physical and chemical properties including high mechanical strengths and ease of processability. Furthermore, the presence of oxygen containing groups (carboxyls, alcohols, and epoxides) on the surface and rim of GO's sheets enables the use of different synthetic pathways for its covalent and noncovalent modification.<sup>[18–23]</sup> The chemical functionalization of GO was amply demonstrated to be a powerful strategy to tune its properties toward desired application in (electro)chemical sensing, energy storage, water and gas purification as well as biomedical technologies.<sup>[24–28]</sup> However, GO exhibits poor electrical characteristics when compared to pristine graphene due to the presence of multiple structural defects and the aforementioned oxygen-containing groups acting as traps and scattering sites for efficient

W. Czepa, S. Witomska  
Faculty of Chemistry  
Adam Mickiewicz University  
Uniwersytetu Poznańskiego 8, 61614 Poznań, Poland

W. Czepa, S. Witomska, A. Ciesielski  
Center for Advanced Technologies  
Adam Mickiewicz University  
Uniwersytetu Poznańskiego 10, 61614 Poznań, Poland

P. Samorì, A. Ciesielski  
Nanochemistry Laboratory  
Institut de Science et d'Ingénierie Supramoléculaires (I.S.I.S.)  
Université de Strasbourg, CNRS, ISIS  
8 allée Gaspard Monge, 67000 Strasbourg, France  
E-mail: samori@unistra.fr; ciesielski@unistra.fr

 The ORCID identification number(s) for the author(s) of this article can be found under <https://doi.org/10.1002/smssc.202300013>.

© 2023 The Authors. Small Science published by Wiley-VCH GmbH. This is an open access article under the terms of the Creative Commons Attribution License, which permits use, distribution and reproduction in any medium, provided the original work is properly cited.

DOI: 10.1002/smssc.202300013

charge transport. Moreover, the GO itself is highly hydrophilic and it can be easily penetrated by solvents molecules causing swelling of the material.<sup>[29]</sup> The phenomena significantly influence the structure and result in worsening of long-cycle performance of the electrode causing low stability.<sup>[30]</sup> Nonetheless, various chemical and physical methods for the GO reduction can be used to restore the conjugation between carbon atoms within GO yielding reduced graphene oxide (rGO). The latter is electrically conducting and it can be used both as electrode or semiconductor for the fabrication of optoelectronics devices.<sup>[31]</sup> Interestingly, the reduction and functionalization of GO can be accomplished simultaneously when molecules bearing primary amines are employed to covalently modify GO via condensation between the oxygen functional groups of GO (mainly epoxides) and NH<sub>2</sub> units of ad hoc molecules. This results in the dramatic decrease of oxygen content and restoration of GO conductivity.<sup>[32,33]</sup> Noteworthy, a moderate amount of oxygen is also desired in carbon-based materials when employed as SC's electrode material, as they provide pseudocapacitive characteristics.<sup>[34,35]</sup> Previous works have been focussed on the influence of oxygen content on SC performance in GO/rGO-based electrodes. Harsh reduction conditions might cause drastic decrease in specific capacitance due to lowered pseudocapacity effect.<sup>[36]</sup> The today's performance of most GO/polymer hybrid materials employed as electrodes in SCs, as quantified by its specific capacitance, amounts typically in the range of 100–300 F g<sup>-1</sup>.<sup>[37–39]</sup> Importantly, the crucial obstacle hampering the practical application of GO-based hybrids in SCs is the low energy density, being usually two orders of magnitudes lower than in case of Li-ion batteries and typically reaching values up to 5–15 Wh kg<sup>-1</sup> in case of aqueous electrolytes.<sup>[40]</sup> Notably, Song and co-workers showed that the use of 1-butyl-3-methyl-imidazolium tetrafluoroborate electrolyte allows a high energy density of 51 Wh kg<sup>-1</sup> to be obtained, demonstrating the high potential of organic electrolytes for widening of the potential window.<sup>[41]</sup> Most of reported examples of GO-based SCs comprise aqueous electrolytes, which are relatively cheap, easily available, and provide good ion conductivity. However, the operating voltage windows of such SCs are limited by the thermodynamic water decomposition at 1.23 V.<sup>[42]</sup> According to theoretical predictions, the use of higher voltage windows, which might be modulated by the choice of the electrolyte, represents appealing strategy toward increased energy density and power density performance of SCs.<sup>[43,44]</sup> In particular, organic electrolytes, including ionic liquids, represent attractive solutions when employed in carbonaceous-based SCs.<sup>[45,46]</sup> Among them, tetraethylammonium tetrafluoroborate (TEABF<sub>4</sub>) exhibits very high conductivity (10.55 mS cm<sup>-1</sup>) and very high oxidation and reduction limiting potentials defining an operative voltage window in the range of -3.0 to 3.6 V.<sup>[47]</sup> Hence, organic electrolytes are particularly suitable for the development of hybrid SCs with excellent performance by mastering both ECDL and PS mechanisms of energy storage.<sup>[48]</sup> To generate new electrode materials mastering both mechanisms, we exploited a supramolecular approach comprising the synthesis of a new thioamide-based polymer (THA) and its grafting to GO yielding GO-THA porous hybrids. The latter have been used as electrode material in symmetric SC devices, displaying gravimetric capacitance as high as 221 and 340 F g<sup>-1</sup> at 1 A g<sup>-1</sup> in 1 M aqueous H<sub>2</sub>SO<sub>4</sub> and 1M TEABF<sub>4</sub> in ACN,

respectively. Moreover, the enlarged operating potential window allowed the achievement of energy density of 94.4 Wh kg<sup>-1</sup>, being several times greater than typical values for carbonaceous SCs (Table S6, Supporting Information).

## 2. Results and Discussions

### 2.1. Synthesis

The thioamide polymer (THA) was synthesized in a three-step reaction. First, modified Hofmann rearrangement was employed to substitute terminal primary amines of 2,2'-(ethylenedioxy) bis(ethylamine) with dithiocarbamate salt by reacting the former with carbon disulfide in basic conditions. Subsequently, dithiocarbamate salt was transformed into diisothiocyanate.<sup>[48]</sup> Finally, the condensation of diisothiocyanate and 2,2'-(ethylenedioxy) bis(ethylamine) yielded the thioamide (THA) polymer. The condensation reaction time was set to 1 h to avoid complete polymerization and therefore insoluble polymer precipitation (**Figure 1**). The as-prepared THA was used to modify GO through the ring opening reaction of GO's epoxide-driven nucleophilic attack of THA's terminal primary amines, as well as the esterification of carboxyl moieties located mainly on the GO sheet edges. The former reaction is accomplished thanks to the tautomerization of active sulfides (thioamide grouping).<sup>[49]</sup> The ratio GO:THA 1:10 (w/w) was applied to maximize the functionalization degree of GO and to avoid formation of nonhomogeneous product.

### 2.2. Characterization

<sup>1</sup>H and <sup>13</sup>C NMR analysis was carried out to attain qualitative information on the chemical structure of THA (**Figure S1**, Supporting Information). <sup>1</sup>H spectra revealed the presence of signals at  $\delta$  7.54 (s, 2H), 3.68–3.44 (m, 12H), and 2.67 (t, NH<sub>2</sub>) which are assigned to secondary amine, ethylene units, and terminal amines hydrogens of THA, respectively. The average molecular weight of the polymer size was estimated as 1958 g mol<sup>-1</sup> by MALDI-TOF with MS detector (**Figure S2**, Supporting Information). Scanning electron microscopy (SEM) and transmission electron microscopy (TEM) studies of the GO-THA hybrid material revealed a dense, homogeneous, wrinkled, porous morphology (**Figure 2** and **S3**, Supporting Information). Such porosity is especially beneficial for the subsequent electrochemical experiments, as it is one of the factors enabling efficient electrolyte ion transportation. Moreover, the energy-dispersive X-Ray (EDX) mapping (**Figure S4**, Supporting Information) showed an even distribution of the heteroatoms (S, N) introduced upon functionalization with the THA polymer.

X-ray photoelectron spectroscopy (XPS) measurements of pristine GO, THA, and GO-THA hybrid were performed to cast further light onto the chemical composition of the materials. The survey spectra confirm the presence of introduced heteroatoms (N, S) into the GO structure (**Figure S5**, Supporting Information) High-resolution C 1s spectrum of GO (**Figure 3a**) exhibited typical peaks at 284.6, 286.4, 287.5, and 288.3 eV corresponding to the C–C, C–O, C=O, and COOH groups, respectively. N 1s and S 2p spectra of THA displayed characteristic peaks confirming its structure along with the emergence of resonance effect according

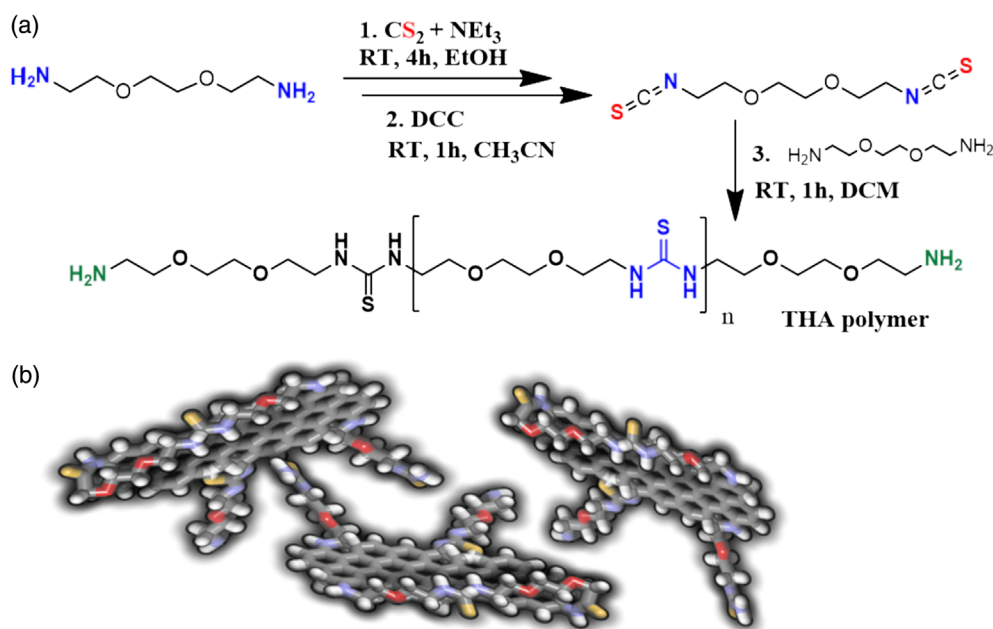


**Figure 1.** a) Scheme of the synthesis of the THA polymer. b) Model of the GO-THA composite.

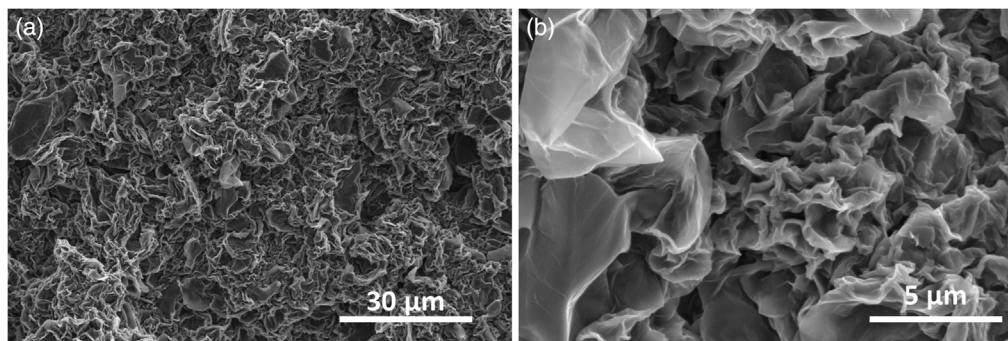


**Figure 2.** SEM images of GO-THA hybrid.

to S 2p high-resolution spectra featuring C=S and C-SH peaks at 161.5 and 163 eV, respectively. (Figure S6, Supporting Information). The C 1s spectra of pristine GO and GO-THA hybrid evidenced major differences. In particular, in the latter two new peaks appeared: the C-N bond (287.3 eV) arising from the covalent attachment of terminal primary amines of THA to GO's epoxides, and the band at 285.5 eV which is assigned to C-S bond and whose presence has confirmed the formation of thioamide.<sup>[50,51]</sup> On the other hand, the N 1s spectra of GO-THA provided valuable insight into the composition of obtained material. While the major peak at 399.5 eV (Figure 3c) can be ascribed to N-C bond of thioamide and secondary amine grouping, the existence of a peak at 398.1 eV is indicative of a resonance effect taking place in the thioamide moiety  $[R1-NH-C(=S)-NH-R2] \leftrightarrow [R1-HN-C(SH)=N-R2]$ .<sup>[52]</sup> The S 2p spectra of GO-THA revealed characteristic sulfur-carbon bonds (at 161.0, 162.1, and 164 eV). Moreover, partial oxidation of sulfides to sulfones was monitored (167.0 and 168.5 eV), occurring simultaneously while functionalizing the

GO. This phenomenon is beneficial especially in view of electrochemical properties of GO-THA, as redox reversible reactions allow the introduction of an additional PS effect and improved the SCs' performance. Notably, the chemical composition of GO-THA hybrid displayed significant degree of functionalization as revealed by a nitrogen and sulfur content amounting to 9.23% and 3.93%, respectively, according to XPS data. Such values are in good agreement with elemental analysis (Table S1, Supporting Information).

Fourier transform infrared spectroscopy (FTIR) spectra of GO and GO-THA are shown in Figure S7, Supporting Information. The GO spectrum displayed the well-known bands at  $1731\text{ cm}^{-1}$  (C=O stretching),  $1620\text{ cm}^{-1}$  (C=C), and stretching of epoxy moieties C-O-C at  $1047\text{ cm}^{-1}$ . Moreover, one can observe the broadband between  $3000\text{ and }3500\text{ cm}^{-1}$ , due to the stretching vibration of the hydroxyl groups. As a result of the functionalization, a strong peak appeared at  $1568\text{ cm}^{-1}$  that can be ascribed to C=N-H stretching vibrations which is characteristic for thiourea resonance structure. Moreover, one can observe

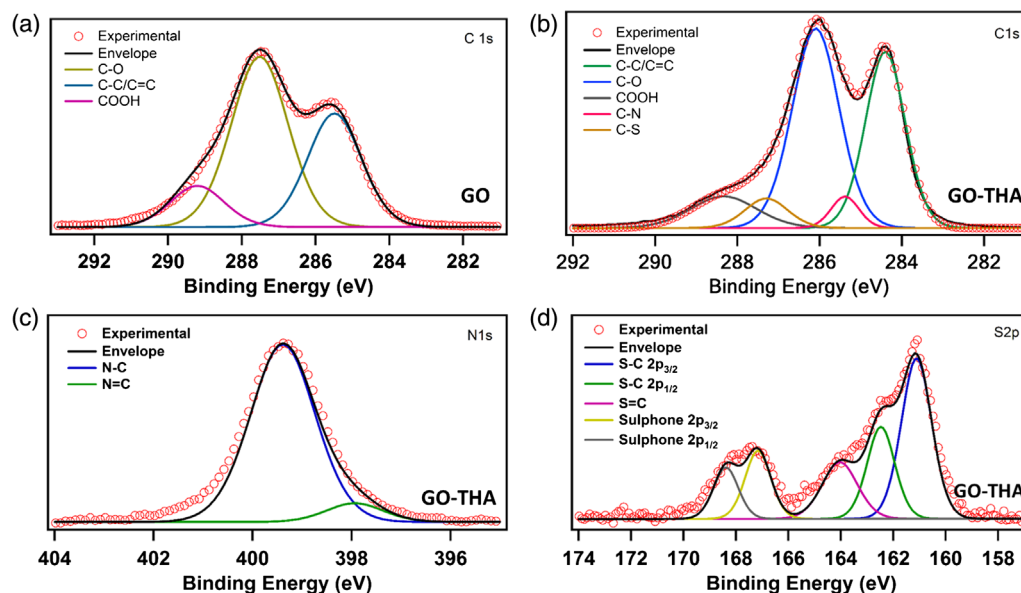


**Figure 3.** High-resolution XPS spectra of GO: a) C 1s, and GO-THA: b) C 1s, c) N 1s, and d) S 2p.

typical  $-\text{CH}_2-$  symmetric and asymmetric stretching at 2864 and 2923  $\text{cm}^{-1}$ , respectively, arising from ethylene grouping present in the polymer.

The functionalization of GO with THA yielded a threefold increase in the specific surface area of 371  $\text{m}^2 \text{g}^{-1}$  according to Brunauer–Emmett–Teller (BET)  $\text{N}_2$  adsorption–desorption investigations (Table S2, Supporting Information). The hysteresis of type H3 (Figure S8, Supporting Information) indicates the slit-like mesopores being present in the material, which is in correlation with an average pore diameter of 3.1 nm. Powder X-ray diffraction (XRD) investigations were performed to study the crystallinity of the materials. Wide-angle X-ray scattering (WAXS) of the pristine GO displayed only the (002) reflection of stacked GO sheets which appears as a typical sharp peak at  $\approx 10.01^\circ$  (see Figure S9, Supporting Information), indicating an interlayer spacing of 0.87 nm, in accordance with previously reported values.<sup>[53,54]</sup> Conversely, the THA polymer exhibited two broad peaks at  $\approx 22^\circ$  and a secondary peak at  $\approx 8.3^\circ$ . Interestingly, GO-THA hybrid featured a peak at  $\approx 8.15^\circ$ , suggesting an increased interlayer spacing between adjacent GO sheets up to 1.05 nm. Moreover, due to functionalization a new broad peak at  $23.4^\circ$  originating from an amorphous THA phase can be identified. Raman spectroscopy provided useful information on the quality and degree of functionalization of GO within GO-THA hybrid. The relative ratio between D and G peaks of GO and GO-THA (Figure S10, Supporting Information), which are located around 1350 and 1600  $\text{cm}^{-1}$  respectively, confirms the highly efficient functionalization. In particular, the increase in the  $I_D/I_G$  ratio from 0.87 to 1.14 in GO-THA reflects the enhancement in structural and electronic disorder after grafting THA polymer, which is due to the enhancement in the  $sp^3$  carbon atoms content in the hybrid, in line with previous reports on GO functionalization.<sup>[55,56]</sup> Thermogravimetric analysis was performed to investigate thermal stability of GO, THA polymer, and GO-THA. The GO curve displayed  $\approx 45\%$  weight loss in the range of 150–300  $^\circ\text{C}$  due to the degradation of oxygen functional

groups. THA exhibited an average thermal stability up to 210  $^\circ\text{C}$ , typical for organic compounds, with a rapid decomposition and weight loss of 60%. The GO-THA curve revealed a slight mass decrease over 100  $^\circ\text{C}$  associated with surface water removal, along with a slow degradation over 150  $^\circ\text{C}$  eventually up to 48% mass loss. Overall, based on the thermal gravimetric analysis (TGA) analysis the relative mass composition of GO-THA is estimated as 80:20 GO:THA (Figure S11, Supporting Information).

### 2.3. Electrochemical Studies

The electrochemical performance of the developed material when integrated in 2-electrodes SC devices was investigated in solid state symmetric setup embedded in CR2030 coin cell. The use of aqueous electrolyte (1M  $\text{H}_2\text{SO}_4$ ) provided excellent wettability mainly due to presence of numerous electronegative atoms (O, N, S) in GO-THA hybrid. The electrolyte–material interface displayed a good conductivity, reaching values of 140  $\text{S cm}^{-1}$  (Figure S12a, Supporting Information). The most important electrochemical characteristic is portrayed in **Figure 4**: the displayed cyclic voltammetry (CV) profile exhibits very good electrode performance. The quasirectangular shape of CV, characterized by small peaks at around 0.4 and 0.5 V, provides evidence for the slight coparticipation of a redox reaction in the energy storage mechanism. The nearly triangular galvanostatic charge–discharge (GCD) curves indicate excellent reversibility and effective charging and discharging of the electrodes. Notably, the electrode does not show any IR drop, which might indicate internal resistance, confirming a negligible charge loss due to resistance effect. Such feature is also confirmed by Nyquist plot revealing solution resistance ( $R_s$ ) and charge resistance transfer ( $R_{CT}$ ) factors of 0.9 and 6.0  $\Omega$ , respectively (Figure 4c). Interestingly, the GO-THA-based device exhibited high specific capacitance of 221  $\text{F g}^{-1}$  at current density of 1  $\text{A g}^{-1}$  combined with a great capacitance retention

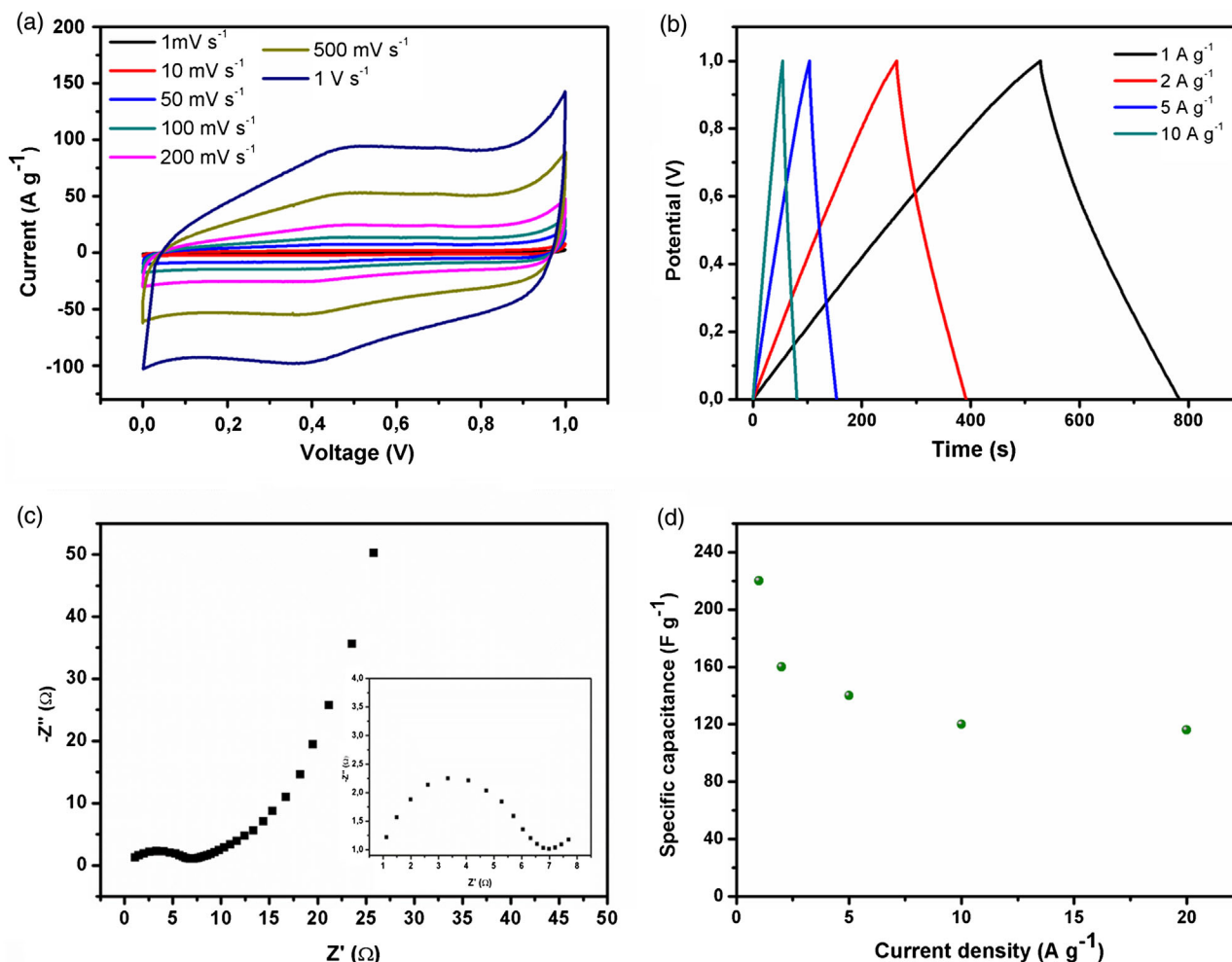


**Figure 4.** Electrochemical characterizations of symmetric SC in 1 M aqueous  $\text{H}_2\text{SO}_4$ : a) CV, b) GCD curves, c) electrochemical impedance spectroscopy, and d) specific capacitance at different current densities.

while increased current density up to  $20 \text{ A g}^{-1}$  ( $120 \text{ F g}^{-1}$ ). Moreover, the stability tests confirmed outstanding performance even after 5000 cycles, with a decrease in the initial capacitance limited to  $\approx 2\%$  (Figure S12b,c, Supporting Information). In general, the operating potential window determines the performance of energy storage devices (Equation (2)). It has been shown that

its widening allows both energy density and power density to be boosted. Toward this end, we have employed 1 M TEABF<sub>4</sub> in acetonitrile as the electrolyte which made it possible to increase the potential window up to 2 V. The CV profiles in Figure 5a show excellent performance, especially in the range of  $2\text{--}500 \text{ mV s}^{-1}$ , as the last curve ( $500 \text{ mV s}^{-1}$ ). Notably, the electrode exhibits

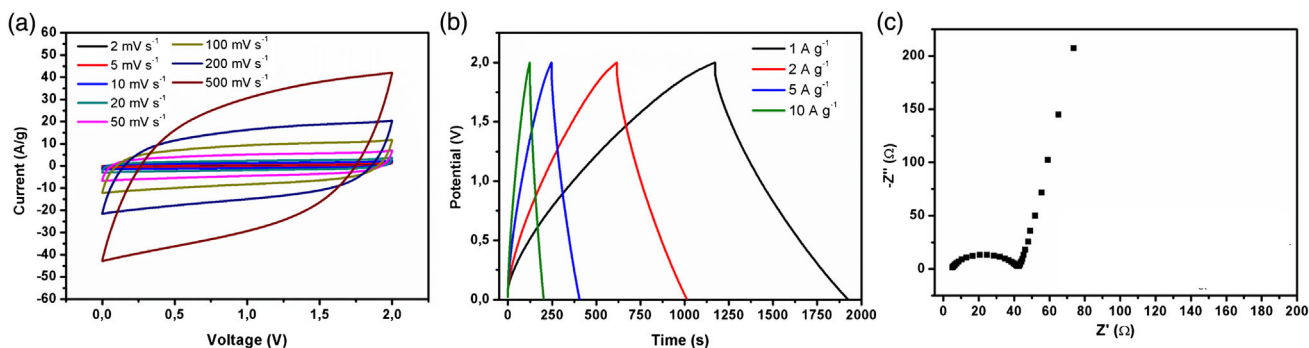


**Figure 5.** Electrochemical characteristics of GO-THA electrodes in 1 M TEABF<sub>4</sub> in ACN: a) CV, b) GCD curves, and c) electrochemical impedance spectroscopy and proposed electrical circuit.

great pseudocapacitive behavior, which can be only observed for low scan rates value (Figure S13, Supporting Information), as the Faradic peaks flatten with subsequent scan rates increment.

The specific capacitance of device calculated from GCD exceeds the value obtained in aqueous media and reaches  $371 \text{ F g}^{-1}$  at current density of  $1 \text{ A g}^{-1}$ , standing out among other GO-related materials (Figure 5b). The electrode also exhibits great capacitance retention at higher current densities reaching  $250 \text{ F g}^{-1}$  at  $20 \text{ A g}^{-1}$  (Figure S14, Supporting Information). Significantly, the increase in the operating window allowed notable increase of the energy density up to values as high as  $94.4 \text{ Wh kg}^{-1}$  with the power density reaching  $333 \text{ mWh cm}^{-3}$ , being exceptional performance for energy storage applications. Moreover, the GO-THA electrodes exhibited high areal and volumetric capacitance of  $556.5 \text{ mF cm}^{-2}$  and  $85.6 \text{ F cm}^{-3}$ , respectively (Table S3, Supporting Information). According to Nyquist plot,  $R_s$  and  $R_{CT}$  factors can be evaluated by fitting the electrochemical impedance spectroscopy (EIS) spectra on the equivalent circuit proposed on Figure S15, Supporting Information. The charge transfer resistance reached values as low as  $32 \Omega$ , thereby providing excellent kinetics of electrochemical processes (Figure 5c). Notably, the attained conductivities of the electrode material correspond to  $48 \text{ S cm}^{-1}$  (Figure S15a, Supporting Information).

### 3. Conclusions

We have demonstrated the covalent functionalization of GO with thioamide-based polymer, as an efficient route to decorate in a robust fashion the surface of GO with different heteroatoms. The multiscale characterization of GO-THA by means of XPS, SEM-EDX, Raman, XRD, and FTIR analysis revealed significant amount of polymer present in the hybrid with high nitrogen and sulfur content. The GO-THA hybrid was employed as electrode material in symmetric SCs that were investigated in both aqueous ( $1 \text{ M H}_2\text{SO}_4$ ) and organic electrolyte ( $1 \text{ M TEABF}_4$  in ACN). In both cases the electrodes exhibited excellent conductivity and very good specific capacitance amounting to 221 and  $340 \text{ F g}^{-1}$ , respectively. Notably, the use of organic electrolyte made it possible to widen the potential window resulting in very high volumetric capacitances of  $85.6 \text{ F cm}^{-3}$  and energy density of  $94.4 \text{ Wh kg}^{-1}$ , being several times higher than typical energy densities of other carbonaceous materials.

### 4. Experimental Section

**Materials:** All the compounds and components required for the synthesis including triethylamine, carbon disulfide, 2,2'-(ethylenedioxy)bis(ethylamine), dicyclohexylcarbodiimide, electrolyte components tetraethylammonium tetrafluoroborate, acetonitrile (electronic grade), separators Whatman glass microfiber filters, binder poly(tetrafluoroethylene), and 1-methyl-2-pyrrolidinone were purchased from Sigma–Aldrich. Conductive carbon black Super P (H30253) was acquired from Alfa Aesar and carbon AvCarb P75 substrate was obtained from FuelCellStore. The GO was acquired from Graphenea ( $4 \text{ mg mL}^{-1}$  solution).

**Synthesis of Polymer THA:** A 4 mL of ethanol was poured into a round bottom glass placed in ice cooled bath and subsequently 3.9 mL of triethylamine (4 eq, 28 mmol) and 4.2 mL of carbon disulfide (10 eq, 70 mmol) were added. Then, 1.04 g of 2,2'-(ethylenedioxy)bis(ethylamine) dissolved in 2 mL of ethanol was droplet added while the reaction mixture was intensively stirred. After 5 min the round bottom glass was taken out from the

ice cooled bath and stored at room temperature for 4 h. Following, a pale-yellow precipitate was filtrated and rinsed with cooled ethanol to yield the final product (yield = 97%). To the solution of  $0.496 \times \text{g N,N}'$ -dicyclohexylcarbodiimide (2 eq, 2.4 mmol) in acetonitrile, 0.68 g of triethylammonium ((ethane-1,2diylbis(oxy))bis(ethane- 2,1-diyl))dicarbamodithiolate (1 eq, 1.2 mmol) dissolved in 5 mL of acetonitrile was added dropwise. The reaction was carried out for 1 h at RT. Subsequently, the white precipitate was filtered, and 10 mL of water was added to the yellow solution, followed by three times extraction with DCM. The combined organic fractions were washed with brine, dried over anhydrous  $\text{Na}_2\text{SO}_4$ , and evaporated till fully exsiccated. The crude product was dissolved in a small volume of cold ethyl acetate and placed in the ice bath for 1 h to enable the precipitation of the residual dicyclohexylurea (DCU). After filtration, the solution was evaporated under the vacuum to give the isothiocyanate product as a yellow oil (60% yield).  $0.68 \times \text{g}$  of 1,2-bis(2-isothiocyanatoethoxy)ethane (1 eq, 2.9 mmol) was dissolved in 10 mL of DCM and added dropwise 0.42 mL of 2,2'-(ethylenedioxy)bis(ethylamine) (1 eq, 2.8 mmol) mixed with constant stirring in RT. After 2 h, additional amount of 2,2'-(ethylenedioxy)bis(ethylamine) (0.1 mL) was added and stirred for 15 min. The precipitate was filtered and dried to yield product (30% yield).

**Preparation of GO-THA Hybrid Material:** A mixture of DMF (10 mL) and aqueous GO ( $10 \text{ mL}$ ,  $4 \text{ mg mL}^{-1}$ ) was sonicated for 15 min and then 10 mL of THA polymer in DMF ( $40 \text{ mg mL}^{-1}$ ) was added. The mixture was rigorously stirred overnight and heated at  $90^\circ\text{C}$ . The resulting powder was then filtered and washed several times with DMF and copious amount of water to remove the unreacted THA polymer. The product was then freeze-dried for 24 h under vacuum to obtain black solid foam-like material.

**Characterization Techniques:** FTIR spectra were recorded in the mid-IR range ( $400\text{--}4000 \text{ cm}^{-1}$ ) by using a Perkin Elmer Spectrometer (Spectrum Two) equipped with ATR Diamond. XPS analyses were carried out on a Thermo Scientific KAlpha X-ray photoelectron spectrometer with a basic chamber pressure of  $\approx 10\text{--}9 \text{ mbar}$  and an Al anode as the X-ray source (X-ray radiation of 1486 eV). X-ray powder diffraction (XRD) experiments were conducted on powder specimens using Bruker ASX D8 Advanced equipped with Cu anode with  $K\alpha$  radiation ( $\lambda = 1.5418 \text{ \AA}$ ). Diffraction patterns were collected at room temperature in the scattered angular range between  $6^\circ$  and  $40^\circ$  with an angular resolution of  $0.02^\circ$  per step and a typical counting time 4 of 10 s per step. The specific surface area was measured by using a Micromeritics ASAP 2050 surface area and porosity analyzer. Prior to the BET measurements, the samples were outgassed for 12 h at  $100^\circ\text{C}$ . Adsorption isotherms were calculated for nitrogen adsorption at 77 K and pressures up to 1 bar. SEM characterization was carried out by means of a FEI Quanta 250 FEG instrument with EDX analyses. High-resolution transmission electron microscopy (HR-TEM) was performed with a Hitachi HT7700 transmission electron microscope. TGA decomposition curves are recorded in the range  $25\text{--}700^\circ\text{C}$  operating under nitrogen atmosphere, with a thermal step of  $10^\circ\text{C min}^{-1}$  on a Mettler Toledo TGA/SDTA851e system. Raman spectra were recorded by a Renishaw microscope with a  $100\times$  objective, laser excitation wavelength of 532 nm, and laser power of 0.05%. The silicon peak at  $520.3 \text{ cm}^{-1}$  was taken as reference for wavenumber calibration. Point of zero charge of adsorbent was determined following previously reported method. Mass spectra were collected on MALDI-TOF mass spectra Ultrafle Xtreme Bruker.

**Preparation of SCs:** The working electrodes were prepared by mixing of GO-THA hybrid (80 wt%, 8 mg), carbon black (10 wt%, 1 mg), and poly(tetrafluoroethylene) (PTFE) (10 wt%, 1 mg) in a probe with 1 mL of N-methylpyrrolidone (NMP) and sonicated for 15 min to achieve homogeneous suspension. Consequently, the material was deposited on carbon substrate providing 2 mg of active material per electrode (AvCarb-P75) and dried under vacuum ( $80^\circ\text{C}$ ). The electrodes were assembled in CR2032 coin cell using Whatman glass microfiber filters as a separator and several drops of the given electrolyte, i.e.,  $1 \text{ M}$  aqueous  $\text{H}_2\text{SO}_4$  or  $1 \text{ M}$  tetraethylammonium tetrafluoroborate in acetonitrile.

**Electrochemical Measurements:** The CV study was performed in the range of 0–2 V with scan rates spanning from 2 to  $1000 \text{ mV s}^{-1}$ . GCD curves were recorded from 0–2 V at different current densities

( $1-20 \text{ A g}^{-1}$ ) and used to calculate specific capacitance using following formula<sup>[49]</sup>

$$E = \frac{2 \times I \times \Delta t}{m \times \Delta V} \quad (1)$$

where  $I$  is a current density,  $\Delta t$  is the discharge time,  $m$  is a mass of the electrode, and  $\Delta V$  is a potential window. EIS and conductivity of electrodes were taken in the frequency range from 200 kHz to 1 mHz with an amplitude of 10 mV. The energy density (Equation (2)) and power density (Equation (3)) were calculated as given

$$E = \frac{C \times \Delta V^2}{3.6 \times 2} \quad (2)$$

$$P = \frac{E'}{\Delta t} \times 3600 \quad (3)$$

where  $E$  is the energy density ( $\text{Wh kg}^{-1}$ ),  $C$  is the gravimetric capacitance,  $\Delta V$  is the discharge voltage range,  $P$  is the power density (in  $\text{mWh cm}^{-3}$ ),  $E'$  is the volumetric energy density, and  $\Delta t$  is the discharge time. CVs, GCD curves, and EIS were recorded using EC-LAB VMP3 (BioLogic Science Instrument).

## Supporting Information

Supporting Information is available from the Wiley Online Library or from the author.

## Acknowledgements

This work was financially supported by the National Science Center (grant nos. 2019/33/N/ST5/00052 and 2019/35/B/ST5/01568). Grant no. POWR.03.02.00-00-1026/16 co-financed by the European Union through the European Social Fund under the Operational Program Knowledge Education Development. The authors also acknowledge support from the Interdisciplinary Thematic Institute SysChem via the IdEx Unistra (ANR-10-IDEX-0002) within the program Investissement d'Avenir program, the Fondation Jean-Marie Lehn, and the Institut Universitaire de France (IUF).

## Conflict of Interest

The authors declare no conflict of interest.

## Data Availability Statement

The data that support the findings of this study are available from the corresponding author upon reasonable request.

## Keywords

energy storage, graphene oxide, supercapacitors, thioamide polymer

Received: February 6, 2023

Revised: March 16, 2023

Published online: April 5, 2023

- [1] C. Couly, M. Alhabeb, K. L. Van Aken, N. Kurra, L. Gomes, A. M. Navarro-Suárez, B. Anasori, H. N. Alshareef, Y. Gogotsi, *Adv. Electron. Mater.* **2018**, *4*, 1700339.  
[2] J. Sun, B. Luo, H. Li, *Adv. Energy Sustain. Res.* **2022**, *3*, 2100191.

- [3] L. Wang, X. Feng, L. Ren, Q. Piao, J. Zhong, Y. Wang, H. Li, Y. Chen, B. Wang, *J. Am. Chem. Soc.* **2015**, *137*, 4920.  
[4] S. Huang, X. Zhu, S. Sarkar, Y. Zhao, *APL Mater.* **2019**, *7*, 100901.  
[5] C. Lethien, J. Le Bideau, T. Brousse, *Energy Environ. Sci.* **2019**, *12*, 96.  
[6] E. Frackowiak, Q. Abbas, F. Béguin, *J. Energy Chem.* **2013**, *22*, 226.  
[7] R. Guo, L. Li, B. Wang, Y. Xiang, G. Zou, Y. Zhu, H. Hou, X. Ji, *Energy Storage Mater.* **2021**, *37*, 8.  
[8] H. Wu, Y. Zhang, L. Cheng, L. Zheng, Y. Li, W. Yuan, X. Yuan, *Energy Storage Mater.* **2016**, *5*, 8.  
[9] J. Zhu, L. Wang, X. Gan, T. Tang, F. Qin, W. Luo, Q. Li, N. Guo, S. Zhang, D. Jia, H. Song, *Energy Storage Mater.* **2022**, *47*, 158.  
[10] R. Kumar, S. Sahoo, E. Joanni, R. K. Singh, K. Maegawa, W. K. Tan, G. Kawamura, K. K. Kar, A. Matsuda, *Mater. Today* **2020**, *39*, 47.  
[11] S. Kumar, G. Saeed, L. Zhu, K. N. Hui, N. H. Kim, J. H. Lee, *Chem. Eng. J.* **2021**, *403*, 126352.  
[12] H. Pan, J. Y. Li, Y. P. Feng, *Nanoscale Res. Lett.* **2010**, *5*, 654.  
[13] S. Ghosh, S. Barg, S. M. Jeong, K. Ostrikov, *Adv. Energy Mater.* **2020**, *10*, 2001239.  
[14] Z.-H. Huang, T.-Y. Liu, Y. Song, Y. Li, X.-X. Liu, *Nanoscale* **2017**, *9*, 13119.  
[15] J.-S. M. Lee, M. E. Briggs, C.-C. Hu, A. I. Cooper, *Nano Energy* **2018**, *46*, 277.  
[16] Y. M. Volfkovich, V. E. Sosenkin, A. Y. Rychagov, A. V. Melezhik, A. G. Tkachev, E. N. Kabachkov, V. I. Korepanov, I. I. Khodos, A. Michtchenko, Y. M. Shulga, *Microporous Mesoporous Mater.* **2021**, *319*, 111063.  
[17] R. Zhou, Y. Li, K. H. Lam, *J. Mater. Chem. A* **2021**, *9*, 21302.  
[18] D. R. Dreyer, S. Park, C. W. Bielawski, R. S. Ruoff, *Chem. Soc. Rev.* **2010**, *39*, 228.  
[19] S. Eigler, A. Hirsch, *Angew. Chem. Int. Ed.* **2014**, *53*, 7720.  
[20] A. T. Lawal, *Biosens. Bioelectron.* **2019**, *141*, 111384.  
[21] K. Parvez, S. Yang, Y. Hernandez, A. Winter, A. Turchanin, X. Feng, K. Müllen, *ACS Nano* **2012**, *6*, 9541.  
[22] A. Razaq, F. Bibi, X. Zheng, R. Papadakis, S. H. M. Jafri, H. Li, *Materials* **2022**, *15*, 1012.  
[23] F. Bonaccorso, L. Colombo, G. Yu, M. Stoller, V. Tozzini, A. C. Ferrari, R. S. Ruoff, V. Pellegrini, *Science* **2015**, *347*, 1246501.  
[24] H. Guo, T. Jiao, Q. Zhang, W. Guo, Q. Peng, X. Yan, *Nanoscale Res. Lett.* **2015**, *10*, 272.  
[25] F. Li, X. Jiang, J. Zhao, S. Zhang, *Nano Energy* **2015**, *16*, 488.  
[26] X. Liu, J. Li, X. Wang, C. Chen, X. Wang, *J. Nucl. Mater.* **2015**, *466*, 56.  
[27] D. Pakulski, W. Czepa, S. Witomska, A. Aliprandi, P. Pawluć, V. Patroniak, A. Ciesielski, P. Samorì, *J. Mater. Chem. A* **2018**, *6*, 9384.  
[28] J. Xu, Y. Wang, S. Hu, *Microchim. Acta* **2017**, *184*, 1.  
[29] A. Iakunkov, A. V. Talyzin, *Nanoscale* **2020**, *12*, 21060.  
[30] W. Czepa, S. Witomska, A. Ciesielski, P. Samorì, *Nanoscale* **2020**, *12*, 18733.  
[31] V. Agarwal, P. B. Zetterlund, *Chem. Eng. J.* **2021**, *405*, 127018.  
[32] A. O. E. Abdelhalim, V. V. Sharoyko, A. A. Meshcheriakov, S. D. Martynova, S. V. Ageev, G. O. Iurev, H. Al Mulla, A. V. Petrov, I. L. Solovtsova, L. V. Vasina, I. V. Murin, K. N. Semenov, *Nanomed.: Nanotechnol. Biol. Med.* **2020**, *29*, 102284.  
[33] V. Belessi, D. Petridis, T. Steriotis, K. Spyrou, G. K. Manolis, V. Psycharis, V. Georgakilas, *SN Appl. Sci.* **2018**, *1*, 77.  
[34] K. Gross, J. J. P. Barragán, S. Sangiao, J. M. De Teresa, L. Lajaunie, R. Arenal, H. A. Calderón, P. Prieto, *Nanotechnology* **2016**, *27*, 365708.  
[35] X. Zheng, S. S. Mofarah, A. Cen, C. Cazorla, E. Haque, E. Y. Chen, A. J. Atanacio, M. Manohar, C. Vutukuri, J. L. Abraham, P. Koshy, C. C. Sorrell, *ACS Appl. Mater. Interfaces* **2021**, *13*, 59820.  
[36] Y. J. Oh, J. J. Yoo, Y. I. Kim, J. K. Yoon, H. N. Yoon, J.-H. Kim, S. B. Park, *Electrochim. Acta* **2014**, *116*, 118.  
[37] W. Ge, Q. L. Ma, W. Wang, F. F. Jia, S. X. Song, *Chem. Phys.* **2021**, *543*, 111096.

- [38] M. Hwang, H. W. Kim, J. U. Jin, H. Yoo, J. Yu, B. C. Ku, N. H. You, *Int. J. Energy Res.* **2021**, *45*, 21209.
- [39] B. Rajagopalan, J. S. Chung, *Nanoscale Res. Lett.* **2014**, *9*, 535.
- [40] X. Gao, H. Zhang, E. Guo, F. Yao, Z. Wang, H. Yue, *Microchem. J.* **2021**, *164*, 105979.
- [41] B. Song, J. Zhao, M. Wang, J. Myllavey, Y. Zhu, Z. Geng, D. Chen, Y. Ding, K. Moon, M. Liu, C.-P. Wong, *Nano Energy* **2017**, *31*, 183.
- [42] P. J. McHugh, A. D. Stergiou, M. D. Symes, *Adv. Energy Mater.* **2020**, *10*, 2002453.
- [43] T.-W. Lin, C.-S. Dai, K.-C. Hung, *Sci. Rep.* **2014**, *4*, 7274.
- [44] C. Liu, Z. Yu, D. Neff, A. Zhamu, B. Z. Jang, *Nano Lett.* **2010**, *10*, 4863.
- [45] Q. Wang, J. Yan, Z. Fan, *Energy Environ. Sci.* **2016**, *9*, 729.
- [46] Z. Yang, J. Tian, Z. Yin, C. Cui, W. Qian, F. Wei, *Carbon* **2019**, *141*, 467.
- [47] C. Zhong, Y. Deng, W. Hu, J. Qiao, L. Zhang, J. Zhang, *Chem. Soc. Rev.* **2015**, *44*, 7484.
- [48] X. Wang, Y. Li, F. Lou, M. E. Melandsø Buan, E. Sheridan, D. Chen, *RSC Adv.* **2017**, *7*, 23859.
- [49] X. Shi, S. Zhang, X. Chen, T. Tang, E. Mijowska, *Carbon* **2020**, *157*, 55.
- [50] E. S. Wallis, J. F. Lane, *Org. React.* **2011**, 267.
- [51] Y. Zu, C. He, D. Liu, L. Chen, *Dyes Pigm.* **2020**, *173*, 107841.
- [52] D. Chen, C. Gan, X. Fan, L. Zhang, W. Li, M. Zhu, X. Quan, *Materials* **2019**, *12*, 2800.
- [53] S. Witomska, Z. Liu, W. Czepa, A. Aliprandi, D. Pakulski, P. Pawluć, A. Ciesielski, P. Samorì, *J. Am. Chem. Soc.* **2019**, *141*, 482.
- [54] Y. He, Z. Shan, T. Tan, Z. Chen, Y. Zhang, *Polymers* **2018**, *10*, 930.
- [55] J. Zhang, H. Zhao, G. Li, X. Zhu, L. Shang, Y. He, X. Liu, Y. Ma, M. Szostak, *Org. Biomol. Chem.* **2022**, *20*, 5981.
- [56] S. Chen, J. Zhu, X. Wu, Q. Han, X. Wang, *ACS Nano* **2010**, *4*, 2822.